

Mode locking of spatiotemporally periodic orbits in coupled sine circle map lattices

Gauri R. Pradhan,^{1,*} Nandini Chatterjee,^{2,†} and Neelima Gupte^{3,‡}

¹*Department of Physics, University of Pune, Pune 411007, India*

²*Theunissen Laboratory, Department of Psychology, 3210 Tolman Hall, University of California, Berkeley, California 94720-1650*

³*Department of Physics, Indian Institute of Technology, Madras, Madras 600036, India*

(Received 24 January 2001; published 10 April 2002)

We study the organization of mode-locked intervals corresponding to the stable spatiotemporally periodic solutions in a lattice of diffusively coupled sine circle maps with periodic boundary conditions. Spatially periodic initial conditions settle down to spatiotemporally periodic solutions over large regions of the parameter space. In the case of synchronized solutions resulting from synchronized initial conditions, the mode-locked intervals have been seen to follow strict Farey ordering in the temporal periods. However, the nature of the organization of the mode-locked intervals corresponding to higher spatiotemporal periods is highly dependent on initial conditions and on system parameters. Farey ordering in the temporal periods is seen at low coupling for mode-locked intervals of all spatial periods. On the other hand, stable spatial period two solutions show an interesting reversal of Farey ordering at high values of coupling. Other spatially periodic solutions show a complete departure from Farey ordering at high coupling. We also examine the issue of completeness of the mode-locked intervals via a calculation of the fractal dimension of the complement of the mode-locked intervals as a function of the coupling ϵ and the nonlinearity parameter K . Our results are consistent with completeness over a range of values for these parameters. Spatiotemporally periodic solutions of the traveling wave type have their own organization in the parameter space. Novel bifurcations to other types of solutions are seen in the mode-locked intervals. We discuss various features of these bifurcations. We also define a set of new variables using which an analytic treatment of the bifurcations along the $\Omega=0$ line is carried out.

DOI: 10.1103/PhysRevE.65.046227

PACS number(s): 05.45.-a

I. INTRODUCTION

Dynamical systems with many degrees of freedom show many phenomena which involve the interaction of spatial and temporal degrees of freedom and can demonstrate both organized and turbulent behavior. Examples of organized behavior seen in the case of extended systems include pattern formation in two-dimensional arrays of coupled oscillators [1] and charge density waves [2]. The simplest class of organized structures in extended systems, that of spatiotemporally periodic solutions, occurs quite frequently in laboratory experiments. For example, experimental systems such as coupled oscillator arrays [3–5] and multimode lasers [6], support a number of periodic solutions and traveling wave behavior has been seen in coupled electronic circuits [7] and ring lasers [8].

Spatially extended systems which serve as models of coupled oscillators show a distinct tendency towards mode locking [9]. Coupled oscillators tend to lock into commensurate motion where the ratios of their frequencies is a rational number. A striking example of this behavior is the mode locking seen in Josephson-junction series arrays [10]. It is observed that, just as a single Josephson junction oscillates at a frequency that is proportional to the voltage across the junction, multiple Josephson junctions arranged in one dimension, shunted by load, phase lock strongly and thus oscillate coherently for some value of the parameter, in this

case the capacitance. Yet another physically realisable system where mode locking is observed is an overdamped chain of balls connected by identical springs of random lengths subjected to strong sinusoidal potential and a time dependent forcing. Here it is shown that for sufficiently strong pulses and weak springs, the chain moves an integral number of periods for a range of pulse lengths [11].

Thus, it is evident that the existence of periodic solutions and mode locking play an important role in the behavior of extended systems, especially those which can be modeled using oscillators. Coupled map lattice (CML) models [12] have turned out to be simple and effective paradigms for the study of complex spatiotemporal systems such as the ones described above due to their computational tractability and rich phenomenology. A typical example of a CML, the nearest neighbor future coupled map lattice can be described by the evolution equations

$$x_{n+1}^i = (1 - \epsilon)f(x_n^i) + \frac{\epsilon}{2}[f(x_n^{i+1}) + f(x_n^{i-1})], \quad (1)$$

where x_n^i are the variable values at the site i at the time n , the local dynamics is governed by the map f , and ϵ which lies between 0 and 1 is the strength of the coupling parameter.

We make our choice of the local map to be the sine circle map first introduced by Arnold [9], and defined by the evolution equation

$$\theta_{n+1} = f_{\Omega,K}(\theta_n) = \theta_n + \Omega - \frac{K}{2\pi} \sin(2\pi\theta_n), \quad (2)$$

*Electronic address: gau@physics.unipune.ernet.in

†Electronic address: nanchat@uclink4.berkeley.edu

‡Electronic address: gupte@chaos.iitm.ernet.in

where $0 \leq \theta_n \leq 1$, $0 \leq \Omega \leq 1$, $0 \leq \epsilon \leq 1$, and the map is invertible when the nonlinearity parameter $K < 1$. The parameter Ω is the natural frequency of the system for $K=0$. This map is one of the simplest representations of physical phenomena involving periodic motion and exhibits a rich variety of temporal behavior, namely, periodic, quasiperiodic, and chaotic behavior. As is well known, this system shows mode locking as the parameter K is increased, and exhibits the Arnold tongue structure organized by Farey ordering in the K - Ω parameter space and a complete Devil's staircase of periodic orbits at $K=1$ [9]. Such Devil's staircase structures have been seen in diverse contexts such as the one-dimensional (1D) Ising model with long-range interactions [13], the Frenkel-Kontorova model of atoms on a periodic substrate [14], and the 3D Ising model with competing interactions [15].

CML studies of lattices of coupled sine circle maps [defined in Eq. 3 below] show a remarkable diversity of behavior [16]. Since the system under study has many degrees of freedom, it is highly sensitive to initial conditions [17]. The class of initial conditions that we study is the class of spatially periodic initial conditions. These are a natural class of initial conditions, are easy to excite in an experimental context and result in stable spatiotemporally periodic solutions over a very large region of parameter space. We examine spatially periodic conditions of spatial period k . It has been observed earlier that synchronized initial conditions where $k=1$ settle down to stable synchronized solutions of varying temporal periods Q , and that the Arnold tongue structure and the Devil's staircase seen for the synchronized solutions is exactly the same as that seen for the single circle map [16] and therefore follows the Farey sequence. The widths of the mode locked intervals are found to be independent of the coupling strength ϵ and are identical to those of the temporally periodic orbits of the single circle map. Hence, the completeness of the mode-locked regions over the Ω interval at $K=1$ seen in the case of the single circle map carries over to the stable synchronized solutions resulting from synchronized initial conditions. On the other hand, the question of the organization of the higher spatially periodic orbits and the manner in which mode-locked intervals of such higher spatial periods fill up the parameter space remains open. This is the question addressed in the present paper.

In marked contrast with the synchronized situation, the organization of spatiotemporally periodic orbits which is obtained from the evolution of initial conditions of spatial period $k > 1$ shows distinct departures from Farey organization in large regions of parameter space. The specific nature of the departure depends on the period of the initial conditions evolved with initial conditions corresponding to odd and even periods falling in different classes. For even period $k = 2m, m \geq 1$ initial conditions, the stable spatiotemporally periodic orbits settle down to the spatial periods $m, 2$, or other factors of m with the temporal periods for a given spatial period following the Farey series at low ϵ , whereas they settle down to the spatial period 2 and the temporal orbits show a reversal of the Farey series at high ϵ . Even period initial conditions also settle down to stable solutions with spatial periods corresponding to m or other factors of m

at high ϵ but the temporal periods of these solutions do not follow the Farey sequence. Odd period k initial conditions settle down to spatial periods which correspond to k or its factors, with temporal periods which follow the Farey series at low ϵ with nongeneric departures from the Farey at high ϵ . The organization of spatiotemporal periods is insensitive to perturbations in the spatially periodic initial conditions although the width of the mode-locked intervals can change for large perturbation strengths. The width of the mode-locked intervals corresponding to orbits of spatial period k and temporal period Q (henceforth to be denoted by the notation $SkTQ$) is no longer independent of ϵ and hence the question of the completeness of the mode-locked intervals has to be considered as a function of the parameter ϵ and with reference to specific classes of initial condition. Bifurcations to traveling waves are seen inside many of the mode-locked tongues. These traveling wave solutions have their own characteristic organization in the parameter space which is discussed here. Many other bifurcations which are spatial, temporal, and spatiotemporal in nature can also be observed inside the mode-locked tongues. These bifurcations show several interesting features which we discuss in detail. We also set up an analytic framework by which bifurcations on the $\Omega=0$ line can be picked up.

This paper is organized as follows. In Sec. II we discuss the stability analysis of spatiotemporally periodic solutions. Section III A discusses the role of initial conditions in the spatiotemporal organization of orbits. We discuss the behavior of spatial period two and other odd period solutions in Secs. III C and III D, respectively, the size of the basin of attraction in Sec. III E, and the completeness of the solutions in Sec. III F. We discuss the behavior of traveling waves in Sec. IV. Section V discusses bifurcation behavior. Our results are summarized and discussed in Sec. VI.

II. THE MODEL AND STABILITY ANALYSIS

The model under investigation is a lattice of coupled sine-circle maps with nearest neighbor diffusive coupling and periodic boundary conditions defined by the evolution equation

$$\theta_{t+1}(i) = \left[(1 - \epsilon)f(\theta_t(i)) + \frac{\epsilon}{2}f(\theta_t(i+1)) + \frac{\epsilon}{2}f(\theta_t(i-1)) \right] \pmod{1}, \quad (3)$$

where ϵ is the coupling parameter and i is the index of lattice site and the local map $f(\theta_t)$ is the single sine circle map given by Eq. (2), with parameters as in Eq. (2).

Now consider such a lattice of size kN where k is the spatial periodicity of the solution and N is the number of blocks of the spatial period k . The Taylor series expansion up to first order about any given solution gives a linear stability matrix \mathcal{M}_t^{kN} which is of the order $kN \times kN$. The structure and the eigenvalues of this matrix enable us to determine the stability edge of the corresponding spatiotemporal solution. The general form of the stability matrix at time t will be

$$\mathcal{M}_t^{kN} = \begin{pmatrix} \epsilon_s A_t(1) & \epsilon_n A_t(2) & 0 & 0 & \epsilon_n A_t(kN) \\ \epsilon_n A_t(1) & \epsilon_s A_t(2) & \epsilon_n A_t(3) & \cdots & 0 \\ 0 & \epsilon_n A_t(2) & \epsilon_s A_t(3) & \epsilon_n A_t(4) & 0 \\ \vdots & \vdots & \vdots & \vdots & \vdots \\ \epsilon_n A_t(1) & 0 & \cdots & \epsilon_n A_t(kN-1) & \epsilon_s A_t(kN) \end{pmatrix}, \quad (4)$$

where $\epsilon_s = (1 - \epsilon)$ and $\epsilon_n = \epsilon/2$, and the $A_t(i) = f'(\theta_t(i)) = 1 - K \cos(2\pi\theta_t(i))$.

For a spatially periodic solution with period k , i.e., when $\theta_t(i+k) = \theta_t(i)$, for all i and temporal period 1, the form of the stability matrix in Eq. (4) can be simplified and can be put in a block diagonal form $\mathcal{M}_t'^{kN}$, with N blocks $\mathcal{M}_t^k(l)$, $l = 1, 2, \dots, N$ each of size $k \times k$ along the diagonal [18,16]. For $k > 2$ each of the $\mathcal{M}_t^k(l)$, $l = 1, 2, \dots, N$, has the structure

$$\mathcal{M}_t^k(l) = \begin{pmatrix} \epsilon_s A_t(1) & \epsilon_n A_t(2) & 0 & 0 & \epsilon_n A_t(k) \omega_l \\ \epsilon_n A_t(1) & \epsilon_s A_t(2) & \epsilon_n A_t(3) & \cdots & 0 \\ 0 & \epsilon_n A_t(2) & \epsilon_s A_t(3) & \epsilon_n A_t(4) & 0 \\ \vdots & \vdots & \vdots & \vdots & \vdots \\ \epsilon_n A_t(1) \omega_l^{-1} & 0 & \cdots & \epsilon_n A_t(k-1) & \epsilon_s A_t(k) \end{pmatrix}, \quad (5)$$

where $\omega_l = 2\pi i(l-1)/N$, $l = 1, 2, \dots, N$.

A similar block diagonal form will be achieved for the $k = 2$ case as well but the matrix $\mathcal{M}_t^k(l)$ has a different form given by

$$M_t^2(l) = \begin{pmatrix} (1 - \epsilon) \bar{A}_t^2(1) & \frac{\epsilon}{2} (1 + \omega_l) \bar{A}_t^2(2) \\ \frac{\epsilon}{2} (1 + \omega_l^{-1}) \bar{A}_t^2(1) & (1 - \epsilon) \bar{A}_t^2(2) \end{pmatrix}. \quad (6)$$

The problem of finding the largest eigenvalue of the stability matrix $\mathcal{M}_t'^{kN}$ can be further simplified. It has been shown that the largest eigenvalue of the $k \times k$ block corresponding to $l = 1$, viz., $\mathcal{M}_t^k(1)$ is same as that of the largest eigenvalue of the entire $kN \times kN$ matrix $\mathcal{M}_t'^{kN}$ [19]. Thus the stability of a k period solution can be studied by looking at a single, uniquely identified, $k \times k$ matrix, even for a lattice of size kN . This analysis can be extended to arbitrary temporal periods Q where the largest eigenvalue of the stability matrix $\mathcal{J}^{kN} = \prod_{t=1}^Q \mathcal{M}_t'^{kN}$ is the same as the largest eigenvalue of the matrix $\prod_{t=1}^Q \mathcal{M}_t^k(1)$. The use of these results greatly simplifies the numerical stability analysis which follows as the stability analysis for a lattice of size $M = kN$ can be reduced to the eigenvalue analysis of a single matrix of dimension $k \times k$ [20].

We study the evolution of the Eq. (3) for a class of spatially periodic initial conditions for varying spatial period k . For various spatial period k initial conditions, we fix the nonlinearity parameter K and identify the spatial period k and the temporal period Q solutions, i.e., the solutions which satisfy the closure conditions

$$\theta_t(i) = \theta_t(i+k) \quad (7)$$

and

$$\theta_t(i) = \theta_{t+Q}(i). \quad (8)$$

The periodic solutions under consideration are said to be stable if the largest eigenvalue of the matrix $\prod_{t=1}^Q \mathcal{M}_t^k(1)$ is less than 1, i.e.,

$$|\lambda^{\text{largest}}| < 1. \quad (9)$$

We check the periodicity of the solutions up to the accuracy of 10^{-14} and scan the Ω - ϵ parameter space with the mesh size 10^{-3} while obtaining the various phase plots. To ensure that the solutions are stable, we verify that the eigenvalue λ^{largest} is less than one inside the mode-locked regions. Our main interest is the organization (i.e., the sequence in which the parameter space is filled) of various stable mode-locked periodic solutions. Most of our phase plots are obtained for the value $K = 1$ for the nonlinearity parameter as the mode-locked tongues are widest here.

III. ORGANIZATION OF MODE-LOCKED INTERVALS

A. Initial conditions

Due to the existence of many degrees of freedom our system has multiple coexisting attractors and the dynamical behavior of the evolution Eq. (3) is strongly dependent on the nature of initial conditions [17]. We find that while several classes of initial conditions including random initial conditions can settle down to spatiotemporally periodic solutions, spatially periodic initial conditions settle down to spatiotemporally periodic solutions in large regions of the parameter space. Distinct classes of initial conditions lead to distinct organizations of spatiotemporally periodic behavior in the parameter space. It is therefore useful to study the stable behavior resulting from each type of initial condition class by class. It has been shown that random initial conditions settle down to a spatiotemporally synchronized solution for this model in the $\frac{0}{1}$ and $\frac{1}{1}$ tongues of single sine circle

map [16]. For synchronized initial conditions (spatial period $k=1$, henceforth abbreviated as $S1$), the entire structure of the Devil's staircase and Arnold's tongues lifts off to the third dimension ϵ [16].

Here, we concentrate on spatial period k initial conditions where $k \geq 1$. We study initial conditions that are symmetric on the lattice about 0.5, i.e., in the case of spatial period k initial conditions where a block $\theta(1), \theta(2), \dots, \theta(k)$ is repeated, we have $\theta(i) + \theta(k-i+1) = 1.0$ within each block. These initial conditions lead to stable spatiotemporally periodic solutions in large regions of the parameter space. In addition, the stable mode locked intervals seen for this class of initial conditions are symmetric about $\Omega = 0.5$ and result in interesting bifurcations in the parameter space. We note that spatially periodic initial conditions which do not follow the above restriction also lead to stable spatiotemporally periodic orbits in the parameter space, but their regions of stability in parameter space are much smaller than those resulting from the symmetric initial conditions described above. Moreover the symmetry about $\Omega = 0.5$ is lost when the initial conditions are not symmetric. However, the organization of spatiotemporally periodic orbits in the parameter space which we shall discuss in detail below is the same in both cases. We discuss the size of the basin of attraction of these initial conditions in Sec. III E.

The numerical method followed has been outlined in Sec. II above. Initial conditions of a given spatial period k are evolved, the closure of the resulting spatial and temporal period is verified and the stability of the solution is checked via the eigenvalue of the stability matrix [21]. It is seen that initial conditions of spatial period k settle down to stable spatiotemporally periodic solutions $Sk'TQ$ where the k' are factors of k . Stable solutions corresponding to all factors of k from 1 to k are seen in different regions of the parameter space. It is also seen that the region of parameter space occupied by $S1TQ$ and $SkTQ$ solutions is the largest.

Secondly, the organization of the mode-locked intervals of a given spatial period but of varying temporal periods follows the Farey organization in some parts of the parameter space, but departures from Farey organization are seen in other regions of the parameter space. The numerical results also show that the arrangement and width of the mode-locked intervals varies with initial conditions with the behavior for odd and even period initial conditions falling in different classes. We examine these features in detail in the section below. We also examine the issue of the completeness of the mode-locked intervals and the size of the basin of attraction.

B. Synchronized initial conditions $k=1$

As mentioned earlier, it has been observed that synchronized initial conditions ($k=1$) settle to stable spatially synchronized solutions with temporal periods Q which are organized by the Farey sequence, exactly as in the case of the single circle map [16]. It was seen that the Arnold tongue structure in the $K-\Omega$ space and the Devil's staircase of the winding number P/Q versus the corresponding stability interval $\Delta\Omega(P/Q)$ seen for the single circle map lifts off to the

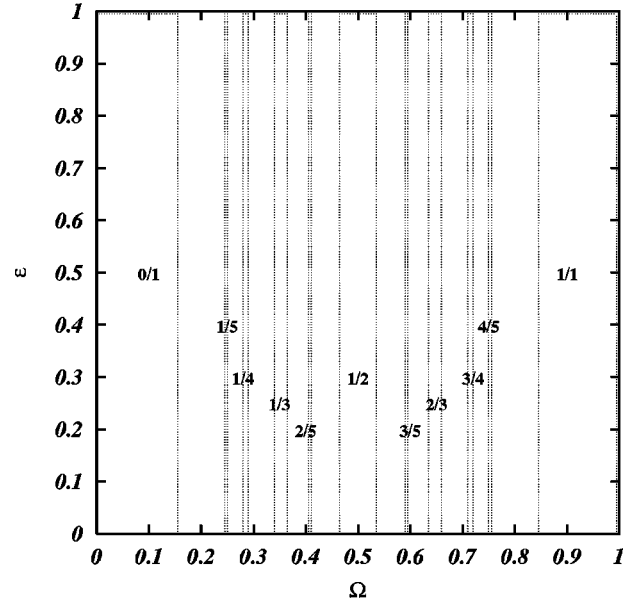


FIG. 1. The mode-locked intervals in the $\epsilon-\Omega$ parameter space corresponding to $S1TQ$ stable solutions arising from $S1$ initial conditions are shown. The width of the intervals is independent of ϵ and the arrangement of the intervals is according to the Farey organization.

third direction, viz. the coupling parameter ϵ [16]. The width of the mode-locked intervals is independent of the coupling strength as seen in the $\epsilon-\Omega$ phase plot in Fig. 1 plotted for $K=1$ with P/Q values as marked in the figure. Thus the completeness of the mode-locked intervals seen in the case of the single sine circle map at $K=1$ carries over to the coupled map as well.

C. Spatial period two initial conditions and initial conditions of even period

Spatial period two initial conditions are the simplest initial conditions of the even period class. The evolution of this class of initial conditions results in stable solutions of spatiotemporal period $S2TQ$ or $S1TQ$. The arrangement of the $S2TQ$ periods in the $\epsilon-\Omega$ plane (for $K=1$) up to $Q=5$ can be seen in Fig. 2(a). It is clear that the mode-locked orbits are arranged in a Farey sequence from $\frac{0}{1}$ to $\frac{1}{1}$ in the lower half plane of ϵ . The P/Q values are as marked in the figure and follow the Farey sequence of order 5 viz. $\frac{0}{1}, \frac{1}{5}, \frac{1}{4}, \frac{1}{3}, \frac{2}{5}, \frac{1}{2}, \frac{3}{5}, \frac{2}{3}, \frac{3}{4}, \frac{4}{5}, \frac{1}{1}$. In contrast the Farey sequence in the upper half-plane follows the order $\frac{1}{2}, \frac{2}{5}, \frac{1}{3}, \frac{1}{4}, \frac{1}{5}, \frac{0}{1} = \frac{1}{1}, \frac{4}{5}, \frac{3}{4}, \frac{2}{3}, \frac{3}{5}, \frac{1}{2}$. This is a reverse Farey sequence which begins and ends at $\frac{1}{2}$. We draw a schematic diagram of this Farey organization and reverse Farey organization in Fig. 2(b). The organization follows the order shown by the solid circle at low ϵ and the dotted circle at high ϵ . Thus there is a beautiful reversal of the Farey sequence in the upper half plane. We have checked numerically temporally mode-locked values upto $Q=64$ and note that the same reversal is seen at all observed levels of the Farey sequence.

We note that that the mode-locked intervals seen in Fig. 2(a) are symmetric about $\Omega = 0.5$ as in the case of the single

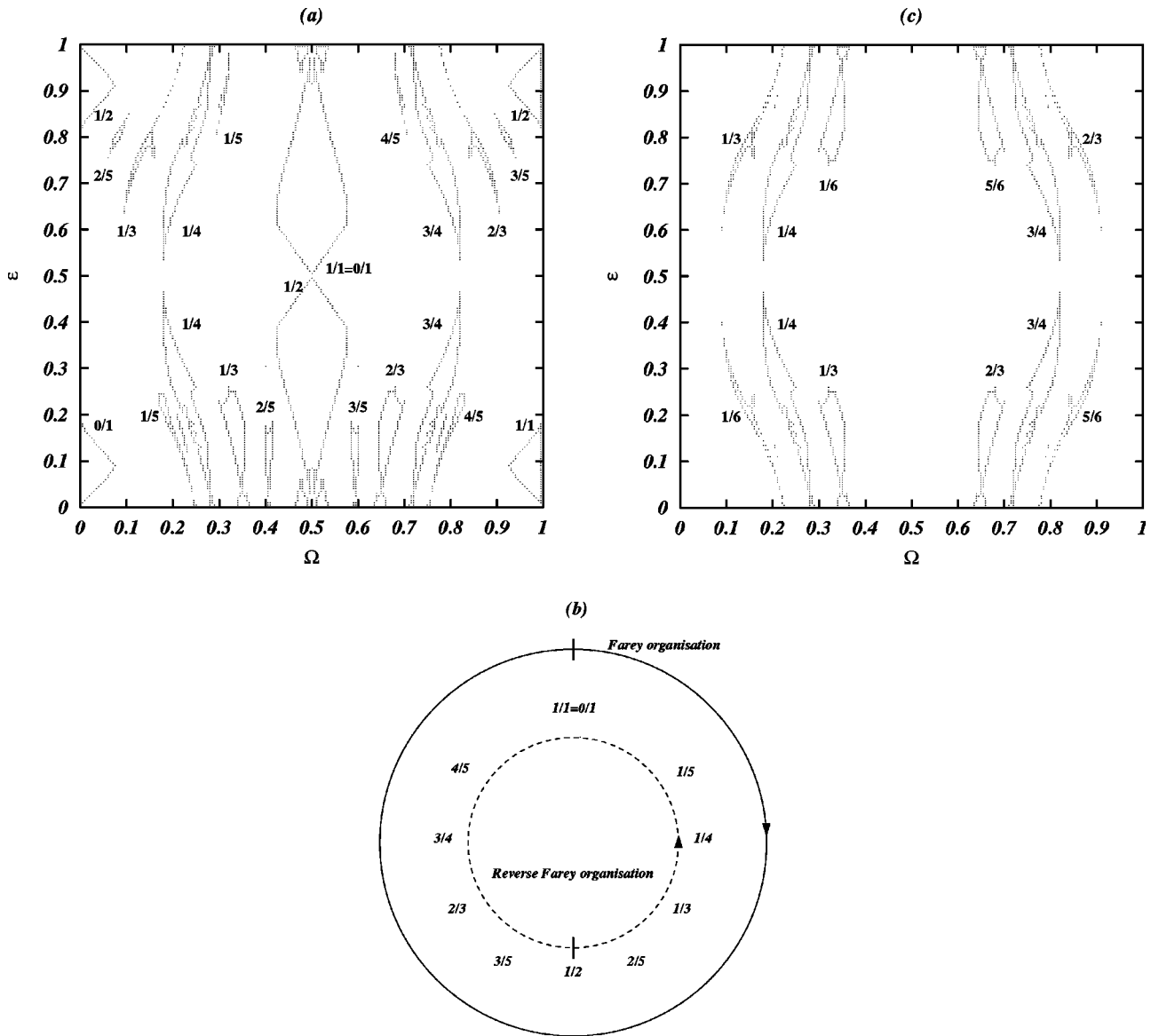


FIG. 2. (a) The mode-locked intervals in the ϵ - Ω parameter space corresponding to $S2TQ$ stable solutions arising from $S2$ initial conditions are shown. The P/Q values are as shown in the figure. The mode-locked intervals are arranged according to Farey series in the lower half plane of ϵ and in the reverse Farey series in the upper half plane of ϵ . (b) The Farey organization starting at $\frac{0}{1}$ and ending at $\frac{1}{1}$ is shown. The points $\frac{0}{1}$ and $\frac{1}{1}$ are identified due to periodic boundary conditions. The starting point and the end point are denoted by vertical bars whereas the arrow gives the direction in which the sequence is traversed. The reverse Farey organization starts at $\frac{1}{2}$ and ends at $\frac{1}{2}$. The arrow on the dotted circle shows the reversal of the direction. (c) The regions of the ϵ - Ω parameter space where $S2TQ$ solutions are stable are shown for the winding numbers $P/Q = \frac{1}{6}, \frac{1}{4}, \frac{1}{3}, \frac{2}{3}, \frac{3}{4}, \frac{5}{6}$. The symmetry in the shapes of the tongues around $\epsilon=0.5$ is clearly seen.

circle map and the synchronized solutions. However the mode-locked intervals resulting from $S2$ initial conditions show an additional symmetry around $\epsilon=0.5$ which is not seen in other cases ($k > 2$) and is not apparent from Fig. 2(a) alone. Mode-locked intervals of winding number P/Q map onto intervals of the same Q when reflected about $\epsilon=0.5$ provided Q is a multiple of 4. If Q is not a multiple of 4, then the interval maps onto an interval of temporal period $Q/2$ or $2Q$ under this symmetry. See Fig. 2(c) which plots mode-locked intervals corresponding to $Q=3,4,6$ where this symmetry is clearly seen. [It is necessary to go to higher tempo-

ral periods to see this symmetry for the mode-locked intervals of Fig. 2(a).]

Now consider spatially periodic initial conditions of higher even periods ($k=2m, m \geq 1$). These initial conditions settle down to stable solutions of spatiotemporal periodicity $Sk'TQ$ where all the factors of k appear as k' , e.g., if the initial condition has spatial period $k=4$, we see stable solutions which are $S4TQ, S1TQ,$ and $S2TQ$. The mode-locked intervals corresponding to these solutions appear in the form of two sets of tongues with bases near $\epsilon=0$ and $\epsilon=1$, respectively. The $S2TQ$ solutions near $\epsilon=1$ appear in the re-

verse Farey sequence as seen in the case of the $S2$ initial conditions above. Near $\epsilon=0.0$, the $S4TQ$ solutions form a complete Farey sequence from $\frac{0}{1}$ to $\frac{1}{1}$. The $S2TQ$ solutions near $\epsilon=0.0$ also form a Farey sequence, but we note that the sequence lacks the two end points $\frac{0}{1}$ and $\frac{1}{1}$ as $S4T1$ solutions are found at these two ends. The combined sequence followed is $\frac{0}{1}, \frac{1}{4}, \frac{1}{4}, \frac{1}{3}, \frac{1}{3}, \frac{1}{2}, \frac{1}{2}, \frac{2}{3}, \frac{2}{3}, \frac{3}{4}, \frac{3}{4}, \frac{1}{1}$, where the denominators of the fractions P/Q correspond to the $S4TQ$ solutions while those P/\tilde{Q} correspond to the $S2TQ$ solutions. Thus elements of the sequence of the lower spatial period 2 always appear to the left of the higher spatial period 4 while $\Omega < 0.5$ with the usual symmetric reversal for $\Omega > 0.5$. Mode-locked intervals corresponding to the $S1TQ$ solutions exhibit Farey organization in temporal periods in all regions of the parameter space.

The entire set of features seen in the case of the spatial period 4 initial conditions discussed here carries over to initial conditions of higher even periods as well. (Even periods have been studied up to $k=14$.) Thus given Sk initial conditions where k is even, the following common features are observed. (i) An $S2TQ$ reverse Farey sequence is seen at high ϵ . (ii) Sk' sequences, where the k' are factors of k are seen with regular Farey ordering at low ϵ . Of these, the $SkTQ$ sequence is complete, whereas the sequences which correspond to other values of k' lack the end points $\frac{0}{1}$ and $\frac{1}{1}$ in a minor violation of Farey ordering. (iii) The elements of the two series merge in a manner in which the Farey ordering is preserved for each $Sk'TQ$ the elements of the sequence with the lower values of the spatial period k' appearing to the left of the higher value of k' . (iv) At high ϵ , spatial periods $k' > 2$ do not show Farey ordering in the temporal periods.

D. Spatial period 3 and other odd spatial period initial conditions

The behavior of stable solutions resulting from odd period initial conditions is quite different from those resulting from the evolution of even period initial conditions. We begin with the study of spatial period $k=3$ initial conditions. The phase plot of the stable mode-locked regions for this set of initial conditions is shown in Fig. 3. It is clear that the mode-locked tongues with bases near $\epsilon=0.0$ follow the regular Farey sequence whereas the mode-locked tongues near $\epsilon=1.0$ clearly violate the Farey sequence. Mode-locked regions resulting from other odd period initial conditions (studied up to $k=15$) show similar behavior, i.e., there is Farey-like behavior at low ϵ whereas nongeneric departures from the Farey are seen at high ϵ .

We note an interesting feature seen in the case of period 3 initial conditions. The Farey sequence between the P/Q values $\frac{1}{3}$ and $\frac{1}{6}$ appears at high ϵ ($0.87 \leq \epsilon \leq 1$) in the Ω range ($0.17 \leq \Omega \leq 0.25$) and a corresponding range to the right of $\Omega=0.5$ by symmetry. No similar feature has been seen in the case of any of the other initial conditions that we have studied.

E. Basins of attraction

We have mentioned above that the condition $\theta(i) + \theta(k-i+1) = 1.0$ is necessary to obtain mode-locked intervals

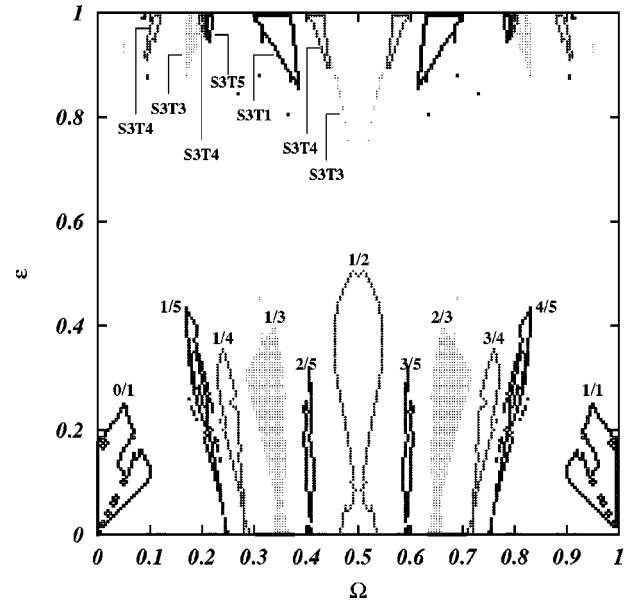


FIG. 3. The mode-locked intervals in the ϵ - Ω parameter space corresponding to $S3TQ$ stable solutions arising from $S3$ initial conditions are shown. The P/Q values are as shown in the figure. The mode-locked intervals are arranged according to Farey series in the lower half plane of ϵ while, unlike $S2$ initial conditions, no specific sequence is seen in the high ϵ regime.

which are symmetric about the $\Omega=0.5$ line but the organization of mode-locked intervals does not depend on this constraint. Other initial conditions of the same spatial period k will result in the same organization of periods but the shapes of the mode-locked regions changes and the symmetry about the $\Omega=0.5$ line is lost. We have also checked that the organization of mode-locked intervals is stable to perturbations. We have added random perturbations of strength 0 to δ to initial conditions of spatial period k and checked the organization of the mode-locked intervals. We note that the organization of mode-locked intervals remains unchanged for perturbations as large as $\delta=0.1$ (i.e., a perturbation strength of 10%) about the spatial period k . The phase space plots after the addition of perturbation remain indistinguishable from the original plots resulting from strictly periodic initial conditions for perturbations up to $\delta=0.001$. However, the shapes of the tongues change for perturbations stronger than this. Thus, the organization of mode-locked intervals is insensitive to fairly strong perturbations to the spatial period of the initial conditions, but the question of completeness of the mode-locked intervals has to be discussed in the context of the specific nature of the initial conditions. We discuss this issue below.

F. The completeness of the mode-locked intervals

In the case of the single sine circle map at the value $K=1$, the width of the mode-locked intervals covers the entire Ω axis and the Devil's staircase of P/Q values against the corresponding stability intervals $\Delta\Omega(P/Q)$ is said to be complete [9]. It is interesting to see if this feature is seen in the case of the coupled sine circle map lattice. From the

previous discussion it is quite clear that the issue of completeness depends strongly on the class of initial conditions and the class of stable solution under consideration. Again, since the width of the mode-locked intervals of a given class depends on the parameter values, the question of completeness has to be studied as a function of the coupling parameter.

In the case of synchronized solutions at $K=1$, as seen above, the width of the mode-locked intervals is independent of ϵ and depends only on Ω [16]. We use the following procedure to investigate the property of completeness for any ϵ . All the plateaus on the Ω axis for which $S1TQ$ solutions are stable are identified upto $Q=95$. The step widths are found up to an accuracy of 10^{-6} . Let $S(r)$ be the total width of the steps which are larger than a given scale r . The space between the steps given by $1-S(r)$ is found for varying r . Then the number of holes is given by $N(r)=[1-S(r)]/r$, if the Ω interval is of unit length. Now, the plot of $\ln N(r)$ versus $\ln(1/r)$ turns out to be a straight line indicating that the power law $N(r)\approx(1/r)^D$ is valid over the Ω interval. Thus the slope of the line gives the dimension D of the set which is complementary to the mode-locked intervals. We have chosen 40 values of r in the interval $(0.000017,0.0009)$ [9]. The dimension D turns out to be 0.876926 ± 0.0008647 . This value is the same for synchronized solutions at all the values of ϵ between 0 and 1. Next we find that for the single circle map, the dimension for the set which is complementary to the mode-locked intervals turns out to be 0.875981 ± 0.0009406 for the same accuracy and the same number of temporal periods and it indeed compares well with the value obtained for the synchronized solutions. Hence we say that the staircase for the synchronized coupled sine circle map lattice is complete for any ϵ . We note that the procedure we have followed is the same as the procedure which has been followed for the single circle map earlier [9] which found $D=0.87$ as the dimension of the complement set of the mode-locked intervals on the Ω axis (where the step width was measured up to an accuracy of 1×10^{-8}).

From the phase plots of the higher spatial periods ($k\geq 2$), it is evident that the widths of the mode-locked regions depend on the coupling strength as well as on the class of initial conditions iterated. Thus the dimension of the complement set of the mode-locked intervals for stable periods $SkTQ$ is a function of the strength of the coupling parameter and also has to be examined for a specific class of initial conditions. We study this quantity using $S2$ initial conditions and find the widths of the mode-locked intervals corresponding to the stable $S2TQ$ solutions. Using the procedure described above, we find the complement set to the mode-locked intervals $S2TQ$ with temporal periods Q up to 95 for different values of the coupling parameter. We plot $\ln N(r)$ against $\ln(1/r)$ in Fig. 4(a) for $\epsilon=0.01$, where all the points fall on a straight line indicating the existence of a power law. The slope gives the dimension $D=0.872159\pm 0.003932$.

It is clear that the width of the mode-locked solutions varies with ϵ for a given K value. We plot $D(\epsilon)$ as a function of ϵ for three K values viz. $K=0.6,0.9,1.0$ in Fig. 4(b). It is clear that for each K value plotted, there is a range of values

of ϵ in the interval $[\epsilon_L, \epsilon_R]$ for which $1-S(r)$ vanishes as r^{1-D} as $r\rightarrow 0$ and therefore, the mode-locked intervals cover the entire Ω axis and the staircase can be said to be complete. At $K=1$ the ϵ_L value is zero indicating that the mode-locked intervals of the single circle map satisfy this property, whereas ϵ_R is about 0.2 after which the curve rises sharply. The behavior of the mode-locked intervals for ϵ values in this range is consistent with completeness. As the value of K decreases, the mode-locked intervals do not fill the Ω axis at $\epsilon=0.0$ and both ϵ_L and ϵ_R shift to the right on the ϵ axis. The value ϵ_{\min} for which the dimension is minimum, D_{\min} shifts to the right as K decreases and the value of D_{\min} decreases as well. The K dependence of these features clearly depends on the way in which the mode-locked tongues open up in parameter space and for $K\leq 0.4$ the completeness property is not seen at any ϵ observed. Similar qualitative behavior is seen at higher spatial periods.

IV. TRAVELING WAVES

Traveling waves (TWs), i.e., waves where the values of the lattice variable translate along the lattice in every time step with a given velocity form an important class of solutions of CMLs [12]. This class of solutions is also found very frequently in experiment [7]. Hence spatiotemporally periodic solutions which have the traveling wave structure deserve special attention [see Fig. 5(a)].

A general spatiotemporally periodic solution with temporal period Q and spatial period k satisfies the condition $\theta_t(i)=\theta_{t+Q}(i+p)$ where $p\text{ mod }k=0$. On the other hand traveling wave solution with spatial period k and temporal period Q which translates with velocity v at each time step clearly satisfies the equation $\theta_t(i)=\theta_{t+Q}(i+vQ)$, where $vQ\text{ mod }k=0$, and the velocity v can take $k-1$ distinct values $1, \dots, k-1$. The TW solution with the velocity k is the frozen solution. Further, the solution with the velocity $k-1$ is the same as that of the solution with velocity 1. For instance, the Fig. 5(a) exhibits this for the TW solutions of spatial period 3 where the velocities admitted are 1 and 2, respectively, with temporal period 3 for both cases. As mentioned earlier, traveling waves of a given spatial period k can have different temporal periods Q and different velocities v which satisfy the relation $vQ\text{ mod }k=0$. For example, the TW solution with the spatial period $k=4$ can have velocities 1, 2, and 3 with the corresponding temporal periods 4, 2, and 4, respectively.

In the case of our CML, spatially periodic initial conditions settle down to spatiotemporally periodic traveling waves in many regions of the parameter space. Moreover, for a fixed value of K , if there is a TW at a given value of (Ω, ϵ) in the $\epsilon-\Omega$ parameter space, then the presence of a TW at $(1-\Omega, \epsilon)$ is guaranteed by symmetry around $\Omega=0.5$. There a definite relation between the velocity v , of TW solutions at these two sets of parameters viz.

$$v_{(\Omega, \epsilon)} + v_{(1-\Omega, \epsilon)} = k. \quad (10)$$

This can be seen clearly from the Fig. 5(b), where the $\epsilon-\Omega$ phase plot at $K=1$ corresponding to stable $S5T5$ TW solu-

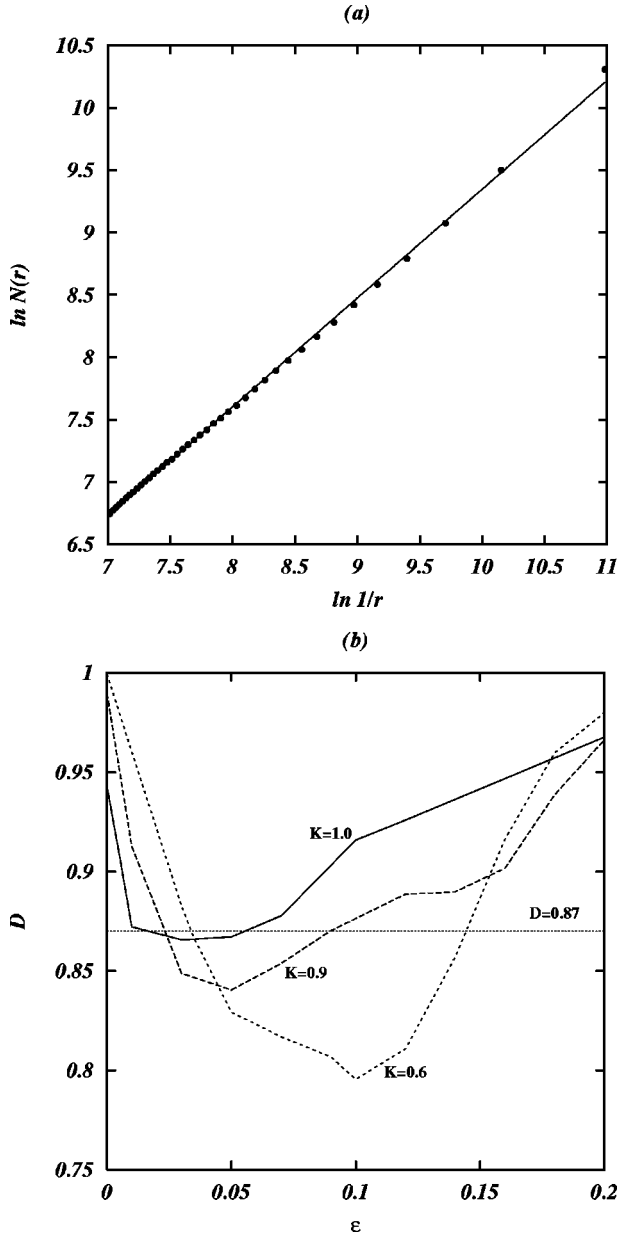


FIG. 4. (a) The plot of $\ln N(r)$ vs $\ln 1/r$ for the coupled sine circle map lattice at $K=1$ and $\epsilon=0.01$ with $S2$ initial conditions. The slope of the straight line gives $D=0.872159 \pm 0.003932$. (b) The dimension of the set complementary to the mode-locked intervals as a function of the coupling parameter for different values of K is plotted. D is seen to vary with the coupling parameter ϵ as shown. Numerical observations show that the staircase is complete over a range of ϵ . The three curves correspond to each of $K=0.6, 0.9$, and 1.0 . The dashed line shows $D=0.87$, the value for the corresponding set for the synchronized solution (at $K=1$) as a reference.

tions with different velocities is shown. The traveling waves with velocities 1, 2, 3, and 4 appear at various parameter values and the relation just described above is satisfied. For example, the TW solution seen in the $\frac{2}{5}$ mode-locked tongue (on left of $\Omega=0.5$) corresponds to the velocity 3 while at the symmetrically opposite position along the Ω axis, on the right of $\Omega=0.5$, the TW solution seen in the $\frac{3}{5}$ mode-locked

tongue corresponds to the velocity 2. (The rest of the tongue contains nontraveling wave solutions. The TW to non-TW bifurcation will be discussed in the next section.)

Further, as in the case of non-TW solutions, spatially periodic initial conditions with spatial period k evolved according to the Eq. (3) settle down to TW solutions with the spatial period k' , where the k' 's are factors of k in different regions of the parameter space. The velocities for the corresponding TW solutions with the spatial period k' follow the relation given by Eq. (10) above. Thus $S4$ initial conditions settle down to $S2T2$ (TW) solutions of velocity 1 in small regimes of $\frac{0}{1}$ and $\frac{1}{1}$ tongues and $S4T4$ (TW) solutions with velocity 1 inside the main $\frac{1}{4}$ tongue while $S4T4$ (TW) solutions with velocity 3 are seen in the $\frac{3}{4}$ tongue in the Ω - ϵ parameter space. Solutions which are traveling waves of the type $S4T2$ are also seen in the $\frac{1}{2}$ tongue. As k increases, and the factors of k increase in number, the widths of the mode-locked intervals decrease.

A. Spatiotemporally periodic staircase: the $k=Q$ case

In the case of a single sine circle map, the intervals $\Delta\Omega(P/Q)$ corresponding temporally mode-locked regions of winding number P/Q form a Devil's staircase. It is therefore interesting to ask whether the spatial and temporal mode-locked regions arising from the spatiotemporally periodic solutions of equal spatial and temporal periods $SkTk$ (i.e., the $k=Q$ case) give rise to a staircaselike structure which could be called a double Devil's staircase since it is doubly periodic (i.e., periodic in both the spatial as well as temporal periods). Unlike the case of the single sine circle map where all the mode-locked tongues arise from a single initial condition, here, it is necessary to consider mode-locked tongues of period $SkTk$, each of which arises from a distinct spatially periodic initial condition Sk . We plot the mode-locked tongues of spatiotemporal period $SkTk$ and also have the TW structure for $K=1$.

It is clear that these mode-locked tongues are also arranged in the Farey sequence [see Fig. 5(c)] and the symmetry around $\Omega=0.5$ is maintained. However, since all even period initial conditions give rise to stable TW solutions of period $S2T2$ in two triangular regions at high ϵ , the staircase is augmented by these two triangles. Due to the fact that each of the mode-locked intervals arise from distinct initial conditions, they can occupy overlapping regions in the Ω - ϵ space, and hence no statement about the completeness of the staircase can be made. We note that mode-locked solutions $SkTk$ which do not have the TW structure also form a double Devil's staircase which follows the Farey series. Additionally, TW solutions arising from the other classes of the spatially periodic initial conditions, e.g., those that are not symmetric about 0.5 also gives rise to the double Devil's staircase but the mode-locked regions reduce in size and the symmetry around $\Omega=0.5$ is lost, however, no overlap between various mode-locked regions is seen for this case.

V. BIFURCATIONS

Many dynamical systems show bifurcation behavior wherein the qualitative nature of the stable solution changes

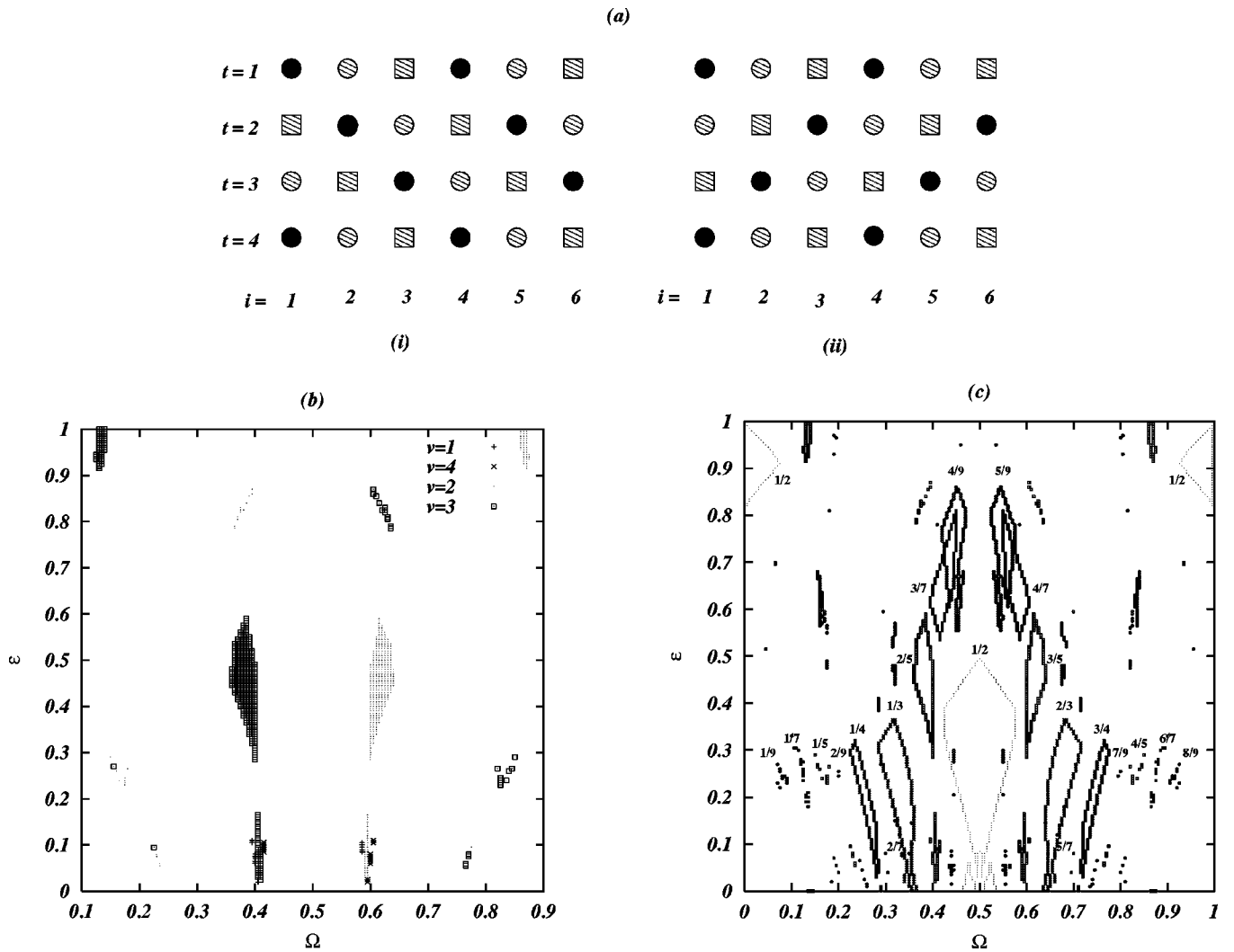


FIG. 5. (a) The traveling wave solutions with spatial as well as temporal period 3 with velocities 1 and 2 are shown in (i) and (ii), respectively. (b) The coupled sine circle map lattice with the $S5$ initial conditions supports the $S5T5$ traveling waves of velocities 1, 2, 3, and 4 following Eq. (10). The regions of stability of these waves are seen in the figure. (c) The stability regions of $SkTk$ traveling wave solutions in the ϵ - Ω parameter space are shown. Each of the $SkTk$ solutions results from the corresponding Sk initial conditions. The P/Q values are as shown in the figure. The spatiotemporally mode-locked regions follow Farey organization. Note the triangles corresponding to the bifurcated solutions in the $\frac{0}{1}$ and $\frac{1}{1}$ tongues.

as the parameters are varied [22]. For low-dimensional systems, these changes are changes in the qualitative temporal behavior of the system. On the other hand, for systems with many degrees of freedom, many attractors with differing spatiotemporal properties are available to the system and bifurcations which are spatial/temporal or spatiotemporal can occur in the system with changes in the parameters [1]. It is clear from the discussion earlier that the model under study shows bifurcations of all types.

It is simplest to discuss bifurcation behavior in the context of the evolution of Eq. (3) for $S2$ initial conditions. Figure 6(a) shows the phase diagram in ϵ - Ω space of the stable solutions resulting from the evolution of $S2$ initial conditions for $K=1$. The triangles seen at low ϵ in the ϵ - Ω parameter space in Fig. 6(a) inside the $\frac{0}{1}$ and $\frac{1}{1}$ tongues, support $S2T1$ solutions while triangles which can be seen in the strong coupling regime, support $S2T2$ (TW) solutions. The $S2T1$

solutions seen in the lower triangles bifurcate to synchronized solutions along the lower edges, and to $S2TQ$ solutions of higher temporal periods Q along the upper edges. The $S2T2$ (TW) solutions seen in the upper triangles bifurcate to synchronized solutions along the upper edges and $S2TQ$ solutions along the lower edges. There is a large tongue with $S2T2$ (TW) behavior near $\Omega = \frac{1}{2}$ below $\epsilon = 0.5$ and an $S2T1$ tongue which is symmetric to this at high ϵ . Bifurcations from $S2T2$ (TW) behavior to $S2T2$ (non-TW) behavior are seen near the base of the lower tongue, whereas bifurcations from $S2T1$ behavior to $S2T2$ (non-TW) behavior are seen at high ϵ .

It is clear that the bifurcations seen here are spatial, temporal and spatiotemporal in nature wherein the change that is seen in the behavior of the stable solution is purely spatial, purely temporal or spatiotemporal. In addition the transition from the traveling wave $S2T2$ solution to the nontraveling

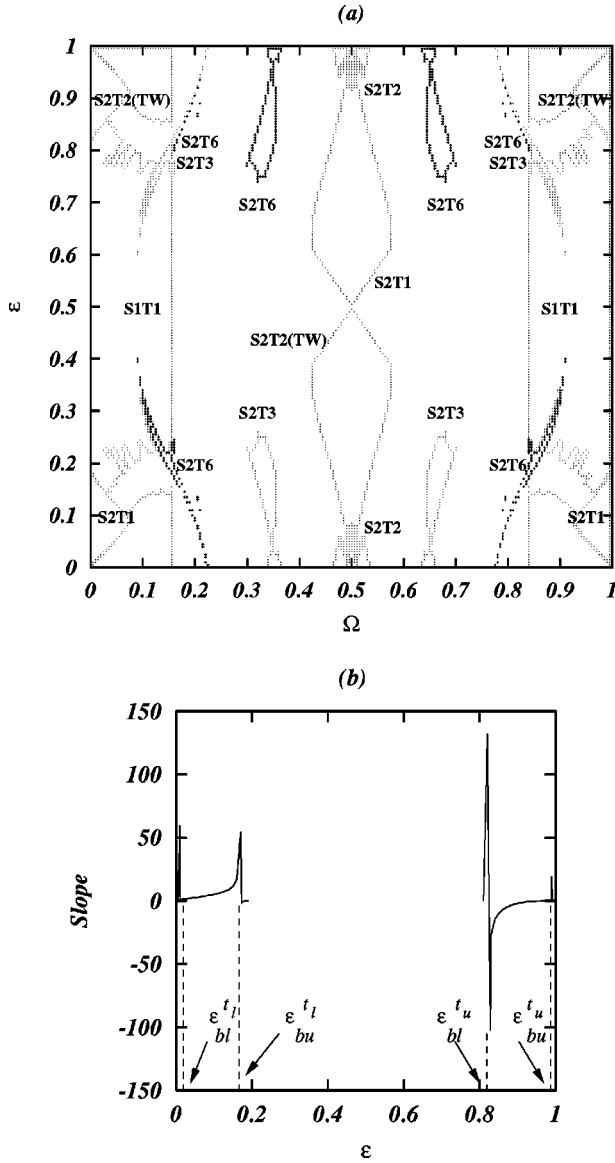


FIG. 6. (a) The ϵ - Ω parameter space corresponding to stable $S2TQ$ and $S1T1$ solutions resulting from $S2$ initial conditions is shown. Clear bifurcation are seen along various edges. The spatiotemporal periods are as marked in the figure. (b) The plot of $d\lambda/d\epsilon$ versus ϵ for $\Omega=0.01$ for the spatially periodic solution resulting from the spatial period 2 initial conditions where λ is the largest eigenvalue. $\epsilon_{bl}^{t_l}$ and $\epsilon_{bu}^{t_l}$ correspond the lower and the upper bifurcation edges of the lower triangle while $\epsilon_{bl}^{t_u}$ and $\epsilon_{bu}^{t_u}$ correspond to the upper triangle in the $\frac{0}{1}$ tongue.

wave $S2T2$ solution is mediated by a spatiotemporal bifurcation by which both the spatial and temporal structures of the initial and final solutions remain the same but the structure of the solution changes from the traveling wave type to the nontraveling wave type. We note that similar bifurcations can be seen in solutions which result from initial conditions of all spatial periods. The bifurcations seen here have several interesting features which we shall discuss in this section. We set up new sum and difference variables and recast the equation of evolution as given by Eq. (3) in a convenient form. We also recast the stability matrix in terms of these

variables. The new variables permit us to cast the analysis in a form where the bifurcation points along the $\Omega=0.0$ line can be picked up analytically. We present this analysis in the subsection below.

A. Analytic evaluation of the bifurcations on the $\Omega=0.0$ line

We consider a lattice of $2N$ sites and construct nearest neighbor differences $\tilde{a}_t(i) = \theta_t(i) - \theta_t(i+1)$ and nearest neighbor sums $\tilde{b}_t(i) = \theta_t(i) + \theta_t(i+1)$. The evolution equation for $\tilde{a}_t(i)$ and $\tilde{b}_t(i)$ are given by

$$\begin{aligned} \tilde{a}_{t+1}(i) = & (1 - \epsilon)[\tilde{h}^a(\tilde{a}_t(i), \tilde{b}_t(i))] \\ & + \frac{\epsilon}{2}[\tilde{h}^a(\tilde{a}_t(i+1), \tilde{b}_t(i+1))] \\ & + \frac{\epsilon}{2}[\tilde{h}^a(\tilde{a}_t(i-1), \tilde{b}_t(i-1))] + p \end{aligned} \quad (11)$$

and

$$\begin{aligned} \tilde{b}_{t+1}(i) = & (1 - \epsilon)[\tilde{h}^b(\tilde{a}_t(i), \tilde{b}_t(i))] \\ & + \frac{\epsilon}{2}[\tilde{h}^b(\tilde{a}_t(i+1), \tilde{b}_t(i+1))] \\ & + \frac{\epsilon}{2}[\tilde{h}^b(\tilde{a}_t(i-1), \tilde{b}_t(i-1))] + 2\Omega + q. \end{aligned} \quad (12)$$

Here,

$$\begin{aligned} \tilde{h}^a(\tilde{a}_t(i), \tilde{b}_t(i)) = & \tilde{a}_t(i) - (K \\ & / \pi) \sin(\pi \tilde{a}_t(i)) \times \cos(\pi \tilde{b}_t(i)) \end{aligned}$$

and

$$\begin{aligned} \tilde{h}^b(\tilde{a}_t(i), \tilde{b}_t(i)) = & \tilde{b}_t(i) - (K \\ & / \pi) \times \sin(\pi \tilde{b}_t(i)) \cos(\pi \tilde{a}_t(i)), \end{aligned}$$

and p and q are integers. We note that since the angle variables $\theta_t(i)$ lie between 0 and 1, the difference variables $\tilde{a}_t(i)$ lie between -1 and 1 and the sum variables $\tilde{b}_t(i)$ lie between 0 and 2.

The closure conditions for the various spatiotemporally periodic solutions seen along the $\Omega=0$ and $\Omega=0.5$ lines, viz $S1T1$, $S2T2$, and $S2T2(TW)$ can be expressed neatly in terms of the new variables $\tilde{a}_t(i)$, $\tilde{b}_t(i)$. The closure conditions for $S2T1$ are given by $\tilde{a}_{t+1}(i) = \tilde{a}_t(i) = -\tilde{a}_t(i+1) \neq 0$ and $\tilde{b}_{t+1}(i) = \tilde{b}_t(i) = \tilde{b}_t(i+1)$. Similarly, the traveling wave solution $S2T2(TW)$ implies the closure conditions $\tilde{a}_{t+1}(i) = -\tilde{a}_t(i) = \tilde{a}_t(i+1) \neq 0$ and $\tilde{b}_{t+1}(i) = \tilde{b}_t(i) = \tilde{b}_t(i+1)$.

We study the stability of different kinds of solutions to the above equations by Taylor expanding the evolution equations

(11) and (12) about the solutions of interest and retaining terms to linear order. The stability matrix so obtained has the form

$$J_t^{4N} = \begin{pmatrix} \tilde{A}_t^{2N} & \tilde{B}_t^{2N} \\ \tilde{B}_t^{2N} & \tilde{A}_t^{2N} \end{pmatrix}, \quad (13)$$

where \tilde{A}_t^{2N} and \tilde{B}_t^{2N} are $2N \times 2N$ matrices which are given by

$$\tilde{A}_t^{2N} = \begin{pmatrix} \epsilon_s \tilde{A}_t(1) & \epsilon_n \tilde{A}_t(2) & 0 & \cdots & \epsilon_n \tilde{A}_t(2N) \\ \epsilon_n \tilde{A}_t(1) & \epsilon_s \tilde{A}_t(2) & \epsilon_n \tilde{A}_t(3) & \cdots & 0 \\ \vdots & \vdots & \vdots & \vdots & \vdots \\ \epsilon_n \tilde{A}_t(1) & 0 & \cdots & \cdots & \epsilon_s \tilde{A}_t(2N) \end{pmatrix}. \quad (14)$$

Here $\epsilon_s = (1 - \epsilon)$, $\epsilon_n = \epsilon/2$ and $\tilde{A}_t(i) = 1 - K \cos[\pi \tilde{a}_t(i) \cos(\pi \tilde{b}_t(i))]$. The matrix \tilde{B}_t^{2N} has a similar form where each $\tilde{A}_t(i)$ is now replaced by $\tilde{B}_t(i)$, where $\tilde{B}_t(i) = K \sin(\pi \tilde{a}_t(i)) \sin(\pi \tilde{b}_t(i))$.

Consider the spatial period 2 solution where $a_t(i) = -a_t(i+1)$ and $b_t(i) = \tilde{b}_t(i+1)$. For these conditions, we find that the matrix \tilde{A}_t^{2N} reduces to a circulant matrix [23] with each $\tilde{A}_t(i) = \tilde{A}_t(1)$, and the matrix \tilde{B}_t^{2N} reduces to a form where $\tilde{B}_t(1) = -\tilde{B}_t(2)$ and $B_t(i) = -B_t(i+1)$.

Using simple matrix algebra, J_t^{4N} can be put into a block diagonal form given by

$$J_t^{4N} = \begin{pmatrix} M_t(+) & 0 \\ 0 & M_t(-) \end{pmatrix}, \quad (15)$$

where $M_t(+) = \tilde{A}_t^{2N} + \tilde{B}_t^{2N}$ and $M_t(-) = \tilde{A}_t^{2N} - \tilde{B}_t^{2N}$. The matrices $M_t(+)$ and $M_t(-)$ are similar [$M_t(-) = \pi M_t(+)$ π^{-1} , where π is the permutation matrix] and thus have the same characteristic polynomial and it is sufficient to consider the eigenvalues of one of them.

We use a similarity transformation which is a direct product of Fourier matrices of size $N \times N$ and identity matrices of size 2×2 which reduces $M_t(+)$ to a matrix of N blocks, each block of size 2×2 [18,23]. For the solution of spatial period two $M_t(l)$ is given by

$$M_t(l) = \begin{pmatrix} (1 - \epsilon)(A + B) & \frac{\epsilon}{2}(1 + \omega_l)(A - B) \\ \frac{\epsilon}{2}(1 + \omega_l^{-1})(A + B) & (1 - \epsilon)(A - B) \end{pmatrix}, \quad (16)$$

where $A + B = \tilde{A}_t(1) + \tilde{B}_t(1)$, $A - B = \tilde{A}_t(1) - \tilde{B}_t(1)$, and $\omega_l = e^{2\pi i(l-1)/N}$ and $l: 1, 2, \dots, N$.

It can be easily seen that the largest eigenvalue occurs for $l = 1, 3, 5, \dots$, and is given by

$$\begin{aligned} \tilde{\lambda} &= (1 - \epsilon)[1 - K \cos \pi \tilde{a}_t(1) \cos \pi \tilde{b}_t(1)] \\ &+ \{ \epsilon^2 [1 - K \cos \pi \tilde{a}_t(1) \cos \pi \tilde{b}_t(1)]^2 \\ &+ (1 - 2\epsilon)[K \sin \pi \tilde{a}_t(1) \sin \pi \tilde{b}_t(1)]^2 \}^{1/2}. \quad (17) \end{aligned}$$

Using the condition that the largest eigenvalue crosses one and the appropriate closure conditions the widths of the ϵ interval for which stable solutions can be obtained. The stability edges for the $\Omega = 0$ and $K = 1$ case can be obtained analytically.

Substituting the S2T1 conditions for this case in Eq. (12) we obtain, for the choice $q = 0$

$$\frac{1}{\pi} \sin \pi \tilde{b}_t(1) \cos \pi \tilde{a}_t(1) = 0 \quad (18)$$

which implies that either $\tilde{b}_t(1) = 0, 1, 2, \dots, n$, and $\tilde{a}_t(i)$ is arbitrary, or $\tilde{a}_t(1) = \frac{1}{2}, \frac{3}{2}, \dots, (2n+1)/2$ and $\tilde{b}_t(i)$ is arbitrary. From Eq. (17) we observe that if the second case is used, the eigenvalue $\tilde{\lambda}$ exceeds 1 and the solution is unstable. Hence for stable S2T1 solutions we use $\tilde{b}_t(1) = 0, 1, 2, \dots, n$, and $\tilde{a}_t(i)$ arbitrary, in Eq. (11) choosing $p = 0$ to get

$$\frac{(1 - 2\epsilon)}{\pi} \sin(\pi \tilde{a}_t(1)) - 2\epsilon \tilde{a}_t(1) = 0. \quad (19)$$

We consider the case where $\tilde{b}_t(1) = 1$ and $\tilde{a}_t(1)$ is arbitrary, a condition also observed in numerical simulations. Using this in Eq. (17), the largest eigenvalue is given by $\tilde{\lambda} = 1 + \cos(\pi \tilde{a}_t(1))$.

For the bifurcation boundary or stability edge of the stable solution, we have $\tilde{\lambda} = 1$ which gives $\tilde{a}_t(1) = \frac{1}{2}, \frac{3}{2}, \dots, (2n+1)/2$. Thus, the stability edge is obtained for $\tilde{a}_t(1) = 0.5 \pmod{1}$. Using this value of $\tilde{a}_t(1)$ in Eq. (19) we find that the stability edge for the S2T1 solution turns out to be $\epsilon = 1/(2 + \pi) = 0.1904$ which is in good agreement with numerical results. Synchronized solutions are seen at $\epsilon = 0$ due to the special nature of the initial condition.

A similar analysis can be carried out for the spatiotemporal bifurcation to traveling wave solutions in the $\frac{0}{1}$ and $\frac{1}{1}$ tongues. The ϵ edges of the S2T2 (TW) solution for $\Omega = 0$ and $K = 1$ can also be analytically obtained using the closure conditions for the S2T2 traveling wave case. In this case the stability matrix J_t^{4N} is replaced by the stability matrix $J_{t+1}^{4N} J_t^{4N}$. Expanding this matrix about the traveling wave solution, it is easy to show that the largest eigenvalue of this matrix is given by $\tilde{\lambda}^2$, so that the stability edge is again given by the condition for the eigenvalue in Eq. (17) crossing 1. Since the conditions on $\tilde{b}_t(i)$ for the traveling wave are the same as those for the S2T1 solution, using arguments similar to those used above, we use $\tilde{b}_t(1) = 0, 1, 2, \dots, n$ and $\tilde{a}_t(i)$ arbitrary in Eq. (11) for the traveling wave to get

TABLE I. The behavior of eigenvalues of the largest modulus at the bifurcation points for $K=1$ in the lower and upper triangles for a fixed Ω in the $\frac{0}{1}$ tongue. Identical behavior is seen in the $\frac{1}{1}$ tongue. ϵ_{bl}^{tl} and ϵ_{bu}^{tl} are the values of ϵ at the bifurcation edge along the lower and upper edges of the lower triangle, respectively, while ϵ_{bl}^{tu} and ϵ_{bu}^{tu} are those at the lower and upper edges of the upper triangle.

$\Omega=0.01$, ϵ values corresponding to the triangle			
	ϵ	Largest eigenvalues	Solution type
$\epsilon < \epsilon_{bl}^{tl}$	0.01	0.00198, 0.00197	S1T1
$\epsilon = \epsilon_{bl}^{tl}$	0.0101	0.00793, 0.00793	S2T1
$\epsilon_{bl}^{tl} < \epsilon < \epsilon_{bu}^{tl}$	0.17	0.8722, 0.8559	S2T1
$\epsilon = \epsilon_{bu}^{tl}$	0.1723897	1.00284, 0.988	S2T1
$\Omega=0.01$, ϵ values corresponding to the upper triangle			
$\epsilon = \epsilon_{bl}^{tu}$	0.8276103	1.0057, 0.52932	S2T2(TW)
$\epsilon_{bl}^{tu} < \epsilon < \epsilon_{bu}^{tu}$	0.83	0.7608, 0.4066	S2T2(TW)
$\epsilon = \epsilon_{bu}^{tu}$	0.9899	0.000062, 0.000031	S2T2(TW)
$\epsilon > \epsilon_{bu}^{tu}$	0.99	0.001975, -0.001936	S1T1
$\Omega=0.5$, ϵ values corresponding to the tips of the small bases inside $\frac{1}{2}$ tongue			
$\epsilon = \epsilon_{bl}$	0.08171	1.0055, 0.87884	S2T2(non-TW)
$\epsilon = \epsilon_{bu}$	0.91829	1.0055, 0.6746	S2T2(non-TW)

$$(1 - \epsilon)\tilde{a}_t(1) + \frac{(1 - 2\epsilon)}{2\pi}\sin(\pi\tilde{a}_t(1)) = 0. \quad (20)$$

Since the stability condition is the same as that above, the stability edge is obtained for $\tilde{a}_t(1)=0.5$. Using this in Eq. (20) we obtain $\epsilon = (\pi + 1)/(2 + \pi) = 0.805523$. We find a close agreement between the analytically and numerically obtained values for $\Omega=0$ and $K=1$. The traveling wave solution is unstable at $\epsilon=1$ as at this value we obtain $\tilde{a}_t(i)=0$ which corresponds to the synchronized solution.

It is thus clear that the bifurcation edges at the lower edge of the upper triangle and the upper edge of the lower triangle can be evaluated by using the condition that the eigenvalue of the stability matrix crosses one and the closure conditions, and that an analytic evaluation of the bifurcation points on the $\Omega=0.0$ line is possible. A numerical evaluation of the bifurcation boundary is necessary at other values of Ω . This throws up some unexpected results which we discuss below.

B. Anomalous behavior of the eigenvalues

We have seen that $S2$ initial conditions settle down to $S2T1$ solutions inside the lower triangles in the $\frac{0}{1}$ and $\frac{1}{1}$ tongues and $S2T2$ traveling waves inside the upper triangles. Synchronized solutions are seen along the lower edge of the lower triangles and the upper edge of the upper triangles. On the other hand, $S2TQ$ solutions are seen along the upper edges of the lower triangles and the lower edges of the upper triangles. We list the largest eigenvalues of the stability matrix observed at these bifurcation edges for $\Omega=0.01$ in Table I.

It is clear from the table that the lower edge of the upper triangle and the upper edge of the lower triangle in the $\frac{0}{1}$ and $\frac{1}{1}$ tongues can be picked up by linear stability analysis with

the largest eigenvalue of the stability matrix crossing one at both these edges, indicating the existence of a tangent bifurcation. However, the upper edge of the upper triangle and the lower edge of lower triangle cannot be picked up by this analysis as the eigenvalue does not cross one in this case even though the nature of the solution changes, from the traveling wave solution to a synchronized solution at the upper triangle, and from an $S2T1$ solution to a synchronized solution at the lower triangle. This situation is exactly like the one seen in the case when kink initial conditions are evolved via Eq. (3) [24], where the bifurcation from the kink solution to the synchronized solution cannot be picked up by the usual eigenvalues. We note that the characterizers set up in the case of the kink case, viz. the rate of change of the largest eigenvalue and the distribution of eigenvalues, work satisfactorily for the present case as well. We plot the rate of change of the largest eigenvalue $d\lambda/d\epsilon$ in Fig. 6(b). It is clear all the bifurcation edges seen in the present case are picked up by the new characterizer [25]. We also note that the bifurcations from $S2T2$ (TW) solutions to $S2T2$ non-traveling wave solutions seen in the $\frac{1}{2}$ tongues are tangent bifurcations which can be picked up by the usual analysis.

As we have seen earlier, the spatial period two solutions resulting from $S2$ initial conditions show a temporal organization which corresponds to the Farey sequence at low ϵ and to a reverse Farey sequence at high ϵ . It is interesting to note that the bifurcation to $S2T2$ traveling waves at high ϵ in the $\frac{0}{1}$ tongue is essential if the reverse Farey organization is to be seen at high ϵ . Similarly, the bifurcation from $S1T1$ to $S2T1$ in the triangles at low ϵ in the same tongues can only be a pure spatial bifurcation as the temporal period must remain unchanged for the usual Farey organization to be followed at low ϵ . Thus the spatial bifurcation along the lower edges in the lower triangles and the spatio temporal bifurcations along

the upper edges of the upper triangles in the $\frac{0}{1}$ and $\frac{1}{1}$ tongues are clearly dictated by the arrangement of the mode-locked regimes in the forward and reverse Farey sequence.

VI. DISCUSSION AND CONCLUSIONS

Thus we have studied the organization of mode-locked intervals in a system of coupled sine circle maps. The organization of the mode-locked intervals is highly sensitive to the nature of the initial conditions and also to the values of the system parameters. The organization corresponding to even and odd period initial conditions falls in different universality classes. Period two initial conditions settle down to mode-locked solutions with spatial period two whose temporal periods show Farey organization at low periods and reverse Farey organization at high periods. Other even period initial conditions result in a systematic organization of stable spatial periods at low ϵ with the temporal organization of each spatial period forming its own Farey, as well as spatial period 2 solutions ordered by the reverse Farey at high ϵ , with other stable spatial periods seen at high ϵ which do not follow the Farey ordering in the temporal periods. The odd spatial periods on the other hand, show Farey organization in the temporal periods at low coupling, but show nongeneric departures from Farey for all the solutions at high coupling. In contrast to the above observations, mode-locked regions corresponding to stable *S1TQ* solutions resulting from both kinds of initial conditions are organized according to the Farey series at all values of coupling. The organization of

mode-locked regions is consistent with completeness over the Ω interval in certain regions of the K - ϵ parameter space. We also see a variety of bifurcations which are purely spatial, purely temporal, and spatiotemporal in various regions of the parameter space. We carry out a systematic study of completeness in the case of mode-locked regions for *S2* initial conditions and identify regions of parameter space where behavior consistent with completeness over the Ω interval is found. We also carry out a systematic study of bifurcations seen in stable solutions resulting from the evolution of *S2* initial conditions. A framework which permits the analytic evaluation of bifurcation points along the $\Omega=0.0$ line at $K=1$ is set up. Additionally we note that all the bifurcations seen here cannot be picked up by the usual quantifiers and define quantifiers which can identify these bifurcations. It is interesting to note that the bifurcations seen in this case are dictated by the fact that the temporal periods at small and large coupling follow forward and reverse Farey organization, respectively. Since our system constitutes a representation of the general behavior of oscillators, it would be interesting to see if some of the behavior seen in our systems can be found in realistic oscillator systems. We hope our analysis will prove to be of utility in some of these contexts.

ACKNOWLEDGMENTS

N.G. thanks DST, India, for partial support under Grant No. SP/S2/E-03/96, and G.R.P. gratefully acknowledges CSIR (India) for financial support.

-
- [1] R. Kapral, Phys. Rev. A **31**, 3868 (1985).
 - [2] J. Levy, M. Sherwin, F. Abraham, and K. Wiesenfeld, Phys. Rev. Lett. **68**, 2968 (1992).
 - [3] K. Wiesenfeld and P. Hadley, Phys. Rev. Lett. **62**, 1335 (1989).
 - [4] M. Choi, H. Kim, D. Kim, and H. Hong, Phys. Rev. E **61**, 371 (2000).
 - [5] H. Hong, M. Choi, K. Park, B. Yoon, and K. Soh, Phys. Rev. E **60**, 4014 (1999).
 - [6] K. Wiesenfeld, C. Bracikowski, G. James, and R. Roy, Phys. Rev. Lett. **65**, 1749 (1990).
 - [7] M. Matias, V. Perez-Munuzuri, M. Lorenz, I. Marino, and V. Perez-Villar, Phys. Rev. Lett. **78**, 219 (1997).
 - [8] M. Clerc and P. Couillet, Phys. Rev. E **60**, 6589 (1999).
 - [9] M.H. Jensen, P. Bak, and T. Bohr, Phys. Rev. A **30**, 1960 (1984).
 - [10] P. Hadley, M. Beasley, and K. Wiesenfeld, Phys. Rev. B **38**, 8712 (1988).
 - [11] S. Coppersmith, Phys. Rev. A **36**, 3375 (1987).
 - [12] K. Kaneko, Chaos **2**, 279 (1992).
 - [13] P. Bak and R. Bruinsma, Phys. Rev. Lett. **49**, 249 (1982); R. Bruinsma and P. Bak, Phys. Rev. B **27**, 5824 (1983).
 - [14] S. Aubry, in *Solitons and Condensed Matter Physics*, edited by A. R. Bishop and T. Schneider (Springer, Berlin, 1978), p. 264.
 - [15] P. Bak and J. von Boehm, Phys. Rev. B **21**, 5297 (1980); M.H. Jensen and P. Bak, *ibid.* **27**, 6853 (1983).
 - [16] N. Chatterjee and N. Gupte, Phys. Rev. E **53**, 4457 (1996); Physica A **224**, 422 (1996).
 - [17] J.F. Heagy, T.L. Carroll, and L.M. Pecora, Phys. Rev. E **50**, 1874 (1994).
 - [18] P.M. Gade and R.E. Amritkar, Phys. Rev. E **47**, 143 (1993).
 - [19] N. Chatterjee and N. Gupte, Phys. Rev. E **63**, 17 202 (2001).
 - [20] However, for most of the cases seen here, the eigenvalue analysis has been carried out for both the $kN \times kN$ and $k \times k$ matrices. The results agree as expected.
 - [21] For initial conditions of spatial period k , the phase plots shown in the figures are for lattices of size $2k$. However, the numerical results have been verified for much larger lattices.
 - [22] J. Guckenheimer and P. Holmes, *Non-linear Oscillations, Dynamical Systems and Bifurcations of Vector Fields* (Springer-Verlag, Berlin, 1983), Chap. 3, p. 117.
 - [23] P. J. Davis, *Circulant Matrices* (Wiley, New York, 1979), Chap. 3, pp. 66–107.
 - [24] G. R. Pradhan and N. Gupte, Int. J. Bifurcation Chaos **11**, 2501 (2001).
 - [25] The distribution of eigenvalues as defined in Ref. [24] above, also picks up all the bifurcations seen, as expected.